Solubility and segregation of B in paramagnetic fcc Fe

Shuang He,[1] Daniel Scheiber,[1] Tobias Jechtl,[1] Franco Moitzi,[1] Oleg Peil,[1] Lorenz Romaner,[1] Sabine Zamberger,[2] Erwin Povoden-Karadeniz,[3] Vsevolod Razumovskiy,[1,*] and Andrei V. Ruban[4]

[1]*Materials Center Leoben Forschung GmbH, Roseggerstraße 12, 8700 Leoben, Austria*

[2]*Voestalpine Forschungsservicegesellschaft Donawitz GmbH, Kerpelystraße 199, 8700 Leoben, Austria*

[3]*Christian Doppler Laboratory for Interfaces and Precipitation Engineering CDL-IPE, Institute of Materials Science and Technology, TU Wien, Getreidemarkt 9, 1060 Vienna, Austria*

[4]*KTH Royal Institute of Technology, SE-100 44 Stockholm, Sweden and Materials Center Leoben Forschung GmbH, Roseggerstraße 12, A-8700 Leoben, Austria*

(Received 29 September 2021; revised 7 February 2022; accepted 8 February 2022; published 28 February 2022)

Boron solubility and segregation in paramagnetic (PM) fcc iron have been investigated by means of DFT calculations. The results focus on the Boron site preference in both bulk and coincidence site lattice model Σ5 (012) GB in fcc Fe and evaluate the validity of different model approaches for modeling the PM state. Boron and PM fcc iron are predicted to form an interstitial solid solution. The PM state model and pressure correction have been introduced into the 0 K DFT calculations to evaluate Boron solubility in fcc Fe as a function of its thermal lattice expansion within the temperature range of 0–1670 K. The relatively high segregation energy of Boron of about −1.57 eV to both interstitial and substitutional GB sites at 0 K is predicted to substantially decrease with thermal lattice expansion, reaching the value of about −0.3 eV at the lattice parameter of fcc Fe corresponding to 1670 K. The contribution of the PM state to the segregation energy was found to be of the order of 0.1 eV compared to the nonmagnetic calculations.

DOI: 10.1103/PhysRevMaterials.6.023604

I. INTRODUCTION

Boron (B) plays an important role as a microalloying element in steel as it can strongly affect its hardenability [1], promote formation of desired and undesired microstructures and phases [martensite, borides, preaustenitic, and austenitic grain boundary (GB) size, etc.] [1–3] as well as affect some critical phenomena like hydrogen embrittlement [4,5]. Boron segregation and solubility in iron has been a topic of numerous studies and remains a disputed topic in literature[1,3,5–15]. Nevertheless, there is little quantitative information about its solubility and segregation on the planar defects, like GB, especially in fcc Fe. From the experimental point of view, the main problem is related to the fact that fcc Fe is unstable at room temperature. At the same time, theoretical *ab initio* investigations of fcc Fe (also often referred to in literature as the γ-Fe or austenite phase) are hampered by its nontrivial magnetism, which is weakly itinerant at low temperatures while it is close to a localized type in fcc Fe at high temperatures where it is stable.

The site occupancy of B in fcc Fe has been investigated before in *ab initio* calculations by Li *et al.* [7] and Ahlawat *et al.* [15]. In both calculations, B was found to occupy octahedral positions. However these calculations have been done for the theoretical lattice constant obtained in the nonmagnetic calculations. Ponomareva *et al.* [16] have calculated solution energies of substitutional (Nb, V) and interstitial (C, N) impurities in γ-Fe at 1200 K using the so-called magnetic sampling method for modeling the paramagnetic state. Their results obtained for the experimental lattice constant are in good agreement with the existing experimental data. This computational approach is, however, rather heavy in application to grain boundaries. Therefore we have chosen a different approach, based on the calculations of the separate magnetic contribution to the solution energies, which cannot be ignored since magnetism of fcc Fe at elevated temperatures becomes of a localized type due to thermal lattice expansion.

In this paper, we address two important questions related to B behavior in γ-Fe at temperatures of its stability: (i) site occupancy in the bulk and (ii) segregation to GBs, in comparison with C and N as a case study. To address the first point, we first investigate the dependence of the equation of state of the pure fcc Fe on the changes in the magnetic state and then calculate the solution energy of interstitial and substitutional atoms of B dissolved in the NM (non magnetic) and PM (paramagnetic) fcc Fe as a function of pressure and volume. As the last step, we calculate B segregation to a special GB in fcc Fe, investigate the effects of the magnetic state and the lattice expansion as well as compare the segregation behavior of B with other solutes such as N and C.

II. METHOD

A. DFT computational details

Total-energy calculations within DFT have been performed by the projector augmented-wave (PAW) method [17] as is implemented in the Vienna *ab initio* simulation package (VASP) [18,19]. The Perdew-Burke-Ernzerhof (PBE) form of the generalized gradient approximation (GGA) [20] has been

*vsevolod.razumovskiy@mcl.at

used for the exchange-correlation energy. The energy cutoff has been set to 500 eV. The Brillouin zone integration has been done using the k-point mesh approximately equivalent to the $24 \times 24 \times 24$ grid [21] for the four-atom conventional fcc cubic unit cell. The energy of the paramagnetic state has been obtained using the spin-wave method [22] with integration over eight q points ($2 \times 2 \times 2$ grid [21]) in the irreducible part of the Brillouin zone.

The magnetic contribution has been obtained by the Green's function exact muffin-tin orbitals (EMTO) [23–25] method which allows disordered local moment (DLM) calculations within the coherent potential approximation (CPA) [26,27]. All the self-consistent EMTO-CPA calculations have been performed by using an orbital momentum cutoff of $l_{\max} = 3$ for the partial waves. The total energies have been obtained using the GGA-PBE functional [20].

B. Solution energies

The solution energy of an interstitial has been computed as [28,29]

$$E_{\text{s-int}} = E(\text{Fe}_\text{N}\text{X}) - E(\text{Fe}_\text{N}) - E(\text{X}), \tag{1}$$

where $E(\text{Fe}_\text{N}\text{X})$ is the total energy of the N-atom Fe supercell containing one solute atom X at an interstitial site and $E(\text{Fe}_\text{N})$ is the total energy of the same supercell without solute atom X. The energy of a solute atom X in its reference state is given by $E(\text{X})$ (0 K equilibrium α-B crystal structure). Constant (zero) pressure supercell (SC) calculations included a complete relaxation of atomic positions, cell volume, and shape. Atomic relaxations have been included in all fixed volume SC calculations.

For a substitutional impurity, the solution energy has been obtained as [30]

$$E_{\text{s-sub}} = E(\text{Fe}_{\text{N}-1}\text{X}) - E(\text{Fe}_\text{N}) - E(\text{X}) + E(\text{Fe}). \tag{2}$$

Here, $E(\text{Fe}_{\text{N}-1}\text{X})$ denotes the total energy of the N-atom Fe supercell where one Fe atom is replaced by solute atom X and the supercell contains only $N - 1$ Fe atoms. $E(\text{Fe})$ is the energy per atom which corresponds to the matrix phase, i.e., $E(\text{Fe}) = E(\text{Fe}_\text{N})/\text{N}$. For all investigated solutes, the octahedral interstitial site is preferred over the tetrahedral site and is used in all subsequent calculations.

C. Grain boundary energy

In this work, we have considered the coincident site lattice (CSL) $\Sigma 5[100](012)$ GB as one of the most well-studied GBs that is often referred to as *representative* as its energy falls in the midrange of the CSL GB energies in the fcc lattice [31–33]. It has been modelled by a GB slab consisting of 40 (EMTO calculations) and 80 (VASP calculations) atoms in the cell with two misoriented grains that join twice due to periodic boundary conditions (see Fig. 1). The GB energy for this setup is [34]

$$\gamma_{\text{GB}} = (E_{\text{GB}} - E_{\text{slab}})/2A, \tag{3}$$

where E_{GB} and E_{slab} are the total energies of the supercell containing the two GBs and the same supercell without GBs. The GB energy is normalized by the GB area A and factor 2 accounts for two GBs in the corresponding supercell. Atomic relaxation has been included in all GB calculations. Volume of the cell has been kept constant, as discussed in Sec. III. In the EMTO calculations of GBs, the atomic sphere radii have been optimized and four additional empty spheres were added to improve the computational accuracy.

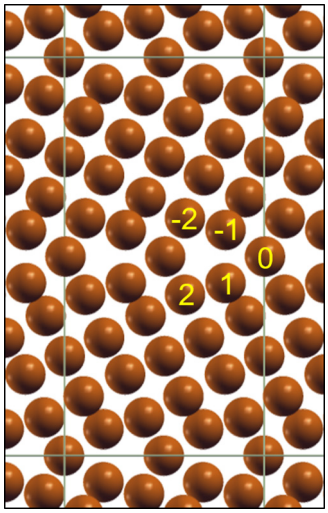

FIG. 1. The structure of the 80-atom $\Sigma 5[100](012)$ GB used in segregation calculations. The numbers label the nearest neighbor layers away from the GB plane (marked as 0).

D. Segregation energies

The GB segregation energy to a specific GB site i, $E_{\text{s}}^{\text{GB,i}}$, is determined as [35,36]:

$$E_{\text{seg}}^{i} = E_{\text{slab}}^{\text{GB,i}} - E_{\text{slab}}^{\text{bulk}}, \tag{4}$$

where $E_{\text{s}}^{\text{GB,i}}$ and $E_{\text{s}}^{\text{bulk}}$ are the total energies of the GB slab with B atoms in the GB sites i and in the most remote from the GB slab layer representing a reference to the "bulk"-like part of the slab.

EMTO calculations have been performed for a 40 atom supercell with B in substitutional positions in the GB and the bulk region in between the GBs as a reference. The atomic positions have been taken from relaxed VASP calculations with a lattice parameter 3.666 Å. The segregation energy difference between 40- and 80-atom slabs with 0.5 monolayers of B has been found to be less than 0.02 eV and therefore a smaller cell was adopted in the EMTO calculations to reduce the computational effort.

III. RESULTS

A. Relative energies of different magnetic structures

Both VASP and EMTO methods have been used to calculate the total energies of fcc Fe in several magnetic states to ensure the equivalence of their results. In particular, we considered ferromagnetic (FM), antiferromagnetic (AFM), double-antiferromagnetic (DAFM), as well as random-paramagnetic (PM) spin structures. The total energy of the PM structure has been calculated by the spin-wave

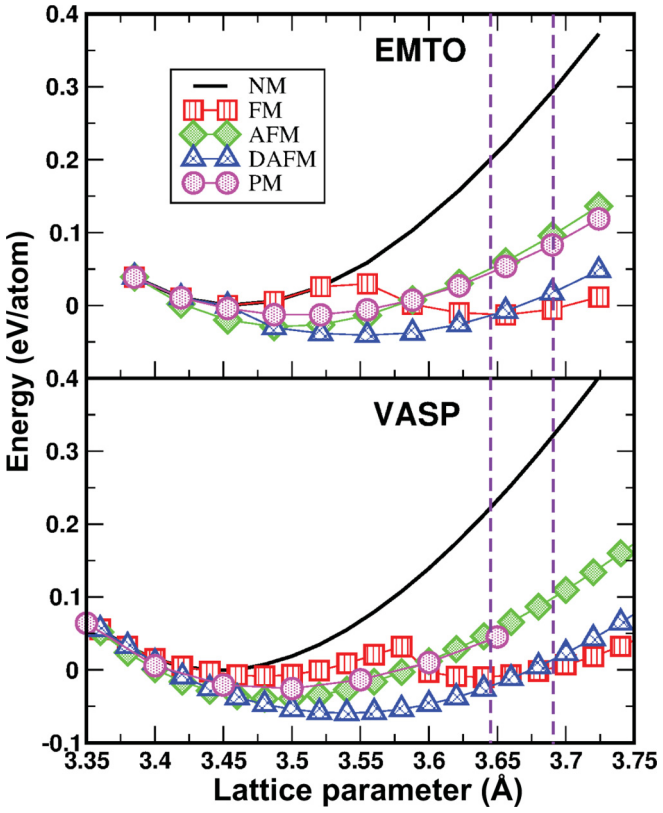

FIG. 2. Energy-volume curves for fcc Fe in different magnetic states obtained in the EMTO and VASP calculations. In both cases, the energies are plotted relative to the NM ground state energy. Dashed lines refer to the range of experimentally measured lattice constants of thermodynamically stable fcc Fe between 1183 and 1670 K [37].

method in VASP and using the DLM set up in the EMTO method. The results are shown in Fig. 2.

The DAFM spin configuration has the lowest energy, which is consistent with other numerous *ab initio* investigations (see, for instance, Refs. [38,39]) where it comes out to be the ground state magnetic structure of the fcc Fe. At the equilibrium lattice constant and below, the energies of different magnetic structures are very close to each other and to the nonmagnetic one. The magnetic moment in this region becomes small and extremely sensitive to the spin configuration, which is a specific feature of a weak itinerant magnet. This leads, for instance, to the double minima total energy curve for the FM spin structure. The second minimum actually lies in the range of the lattice constants of γ-Fe [37] shown by dashed lines in Fig. 2. At these lattice constants, the local magnetic moments of Fe are in the range of 2.0–2.6 μ_B, which is considered to be the so-called "high-spin" state. The local magnetic moment which corresponds to the minimum energy for the corresponding magnetic structure is given in Table I together with the results for the equilibrium lattice constant calculations.

It is interesting to see that the EMTO-CPA DLM and VASP spin-wave energies, which are models for the PM state, are very close to the AFM ones. As one can see in Table I, the local magnetic moments of Fe are also very similar. That means that the AFM structure could be used for modeling of the PM state. The problem, however, is that AFM structure is unstable in the DFT self-consistent supercell calculations when sites, which correspond to the same sublattice in the AFM configuration, become nonequivalent, as would be the case for the GB slab.

TABLE I. The calculated lattice constant (a, Å), magnetic moment per atom (M, μ_B), with literature comparison for fcc Fe.

Magnetic structure	a	M	Method	Ref.
NM	3.446		VASP-PAW	This work
	3.450		VASP-PAW	[40]
	3.460		EMTO-CPA	This work
AFM	3.487	1.33	VASP-PAW	This work
	3.490	1.33	VASP-PAW	[40]
DAFM	3.539	1.93	VASP-PAW	This work
	3.540	1.93	VASP-PAW	[40]
FMLS	3.480	1.00	VASP-PAW	This work
	3.480	0.99	VASP-PAW	[40]
FMHS	3.640	2.59	VASP-PAW	This work
	3.640	2.59	VASP-PAW	[40]
DLM	3.507	1.33	EMTO-CPA	This work
	3.530	0.96	EMTO-CPA	[40]
Spin-wave	3.487	1.30	VASP-PAW	This work

This is the reason why AFM cannot be used in practical supercell calculations, and in this work, we use a different approach, just obtaining the magnetic corrections to the accurate VASP total energies in the NM state from EMTO-DLM calculations for the structure obtained in the VASP calculations. The EMTO method is not precise enough to get the accurate total energy of the open GB structure considered in this work. However, the magnetic energy is mainly related to the change of the one-electron energies and therefore it is much less sensitive to the details of the self-consistent calculations done in this work.

B. Boron solubility in fcc Fe

Boron has a unique ability to form both interstitial and substitutional solid solutions with Fe. There exist several DFT investigations of B solubility in fcc Fe [6,15,41,42]. However, they consider fcc Fe at low temperature lattice constants. Here, we consider the solubility of B in the large lattice constant interval, which also includes the one related to the high-temperature γ-Fe.

First, we calculate the solution energy of B in NM fcc Fe using constant volume and constant pressure conditions at the 0 K equilibrium fcc Fe (see Table I) as a function of the supercell size. The results are shown in Fig. 3. In both cases, the result can be considered as converged for the $4 \times 4 \times 4$ supercell. The solution energy in this case is 0.25 eV for B in the interstitial position and about 0.47 eV in the substitutional case. Thus, B prefers to occupy interstitial positions in NM fcc Fe at 0 K, while it prefers to form the substitutional solid solution at 0 K with the bcc Fe [5].

To obtain the B solution energy in γ-Fe at high temperatures, we introduce two corrections: (i) an effective pressure

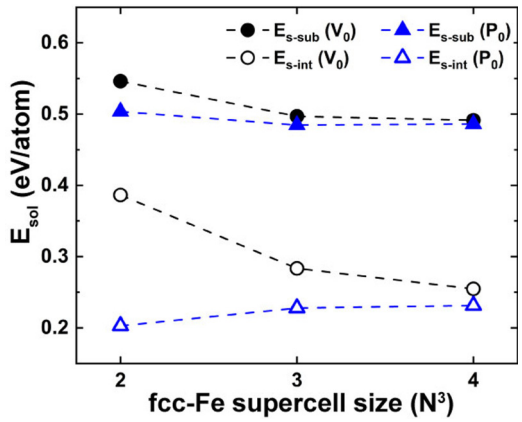

FIG. 3. Solution energy of B as a function of the NM fcc Fe supercell size as an interstitial (top) and as a substitutional (bottom) element. V_0 and P_0 represent the solution energies calculated at constant volume and zero pressure conditions, respectively.

correction to the 0 K DFT calculations, related to the equilibrium volume difference between the 0 K and at $T > 0$ K conditions; (ii) the paramagnetic state energy correction. The effective pressure is obtained in VASP calculations of the solution energy of B at the experimental lattice constants of fcc Fe [37]. Afterwards, the magnetic correction, which is the difference between the PM and NM solution energies at the given pressure, is obtained in the EMTO-CPA calculations.

The results for the solution energies are summarized in Fig. 4 as a function of external pressure. As one can see, the solution energy of B the NM fcc Fe depends very little on the pressure down to −150 kbar (equivalent to the lattice constant of 3.70 Å) and upon contraction up to 25 kbar (equivalent to lattice constant of 3.35 Å). The temperature interval of the thermodynamic stability of the austenite is located between about 1183 and 1670 K, which correspond in our calculations to about −75 and −100 kbar of pressure. Within this range, the solution energy of B in both interstitial and substitutional sites in fcc Fe virtually does not change. The rapidly growing discrepancy between the NM and PM solution energies below −100 kbar is related to the increasing impact of magnetism upon bonding in this pressure range due to larger interatomic distances.

TABLE II. Σ5[100](012) GB energy in fcc Fe in J/m^2. VASP* PM result calculation by an addition of Δ(PM-NM) from EMTO-DLM to the NM VASP result.

Reference	Lattice constant (Å)	NM	PM	Δ (PM-NM)
VASP	3.446	1.60		
VASP	3.666	0.49		
VASP*	3.666		1.19	0.71
EMTO-DLM	3.666	1.63	2.34	0.71
Expt. [44]	3.684		0.8	

The behavior of the solution energies however changes when the magnetic energy contribution is taken into consideration. It has a pronounced nonlinear behavior for both types of sites. In the case of the substitutional alloy, the solution energy increases drastically with decreasing pressure. Almost an inverse behavior is observed in the case of the interstitial B atoms. Thus the interstitial solid solution of B in the fcc Fe becomes more stable relative to the substitutional one as the temperature increases (pressure decreases). However, within the interval of the thermodynamic stability of γ-Fe between 1183 and 1670 K, this change is moderate, about 0.2 eV, and does not change the qualitative picture. This result brings us to a conclusion that NM calculations of the fcc Fe can yield reasonable results for the case of the solution energies, at least for the case of B interstitial atoms, if the temperatures of interest are not too high (see Fig. 4).

C. GB formation energy

The effect of magnetism upon GB formation energy has been investigated using the symmetric CSL Σ5[100](012) GB. As in the case of the solution energies, the fully relaxed NM GB configuration has been calculated in VASP and the magnetic contribution to it has been calculated in EMTO-DLM using the relaxed structure obtained in the NM VASP calculations.

The GB energy calculated with VASP at the 0 K lattice constant is 1.60 J/m^2 for NM fcc Fe (Table II), which agrees well with 1.75 J/m^2 obtained by Li *et al.* [43]. Calculations at a larger lattice constant of 3.666 Å, which is the lattice constant of γ-Fe at about 1400 K [37], yield a significantly reduced GB

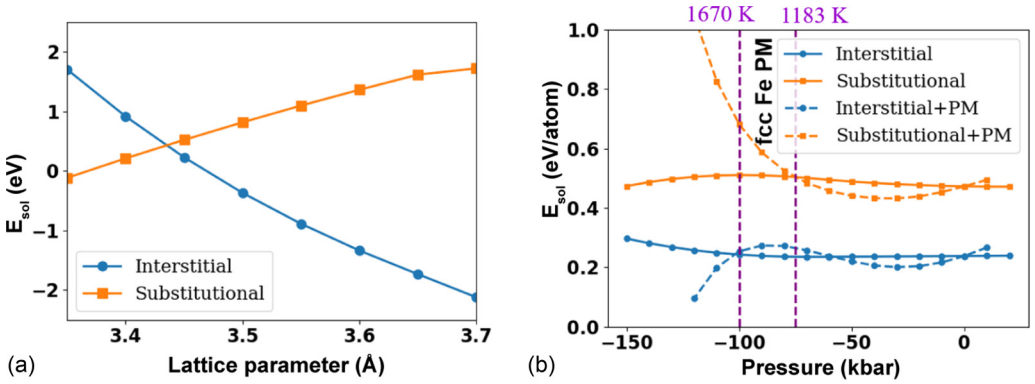

FIG. 4. Solution energy of B (a) as a function of the lattice parameter under equal volume conditions and (b) as a function of pressure for equal pressure conditions for NM fcc Fe. In the case of equal pressure conditions, magnetic energy corrections for the PM state are shown.

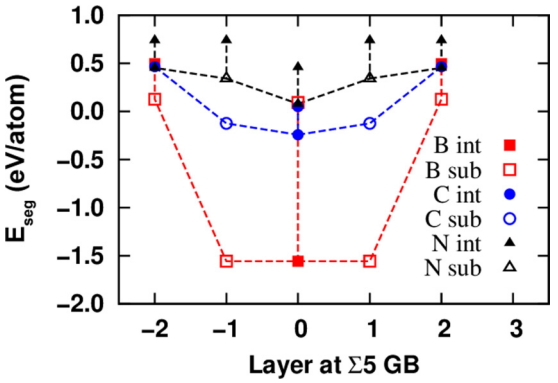

FIG. 5. The segregation energies of B, C, and N to the Σ5[100](012) GB in NM fcc Fe. The numbers label the nearest neighbor layers away from the GB plane (marked as 0).

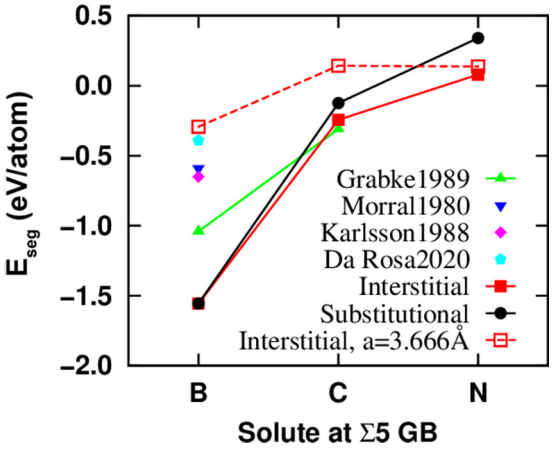

FIG. 6. The minimum segregation energies of B, C, and N at the Σ5[100](012) GB versus experimentally measured segregation energies by Grabke *et al.* [46,48], Morral *et al.* [45], Karlsson *et al.* [47], and Da Rosa *et al.* [11].

energy value of 0.49 J/m^2. The NM EMTO calculations of the fcc GB at 3.666 Å yield 1.63 J/m^2. This overestimation of the GB energy is related to the methodological aspects of the EMTO calculations for relatively open structures as has been discussed above. However, the magnetic energy should be much less affected due to cancellations of errors and its general insensitivity to the methodological differences between the VASP and EMTO calculations.

The PM EMTO-DLM calculations at 3.666 Å yield the GB formation energy of 2.34 J/m^2, which is 0.71 J/m^2 higher than that of the NM state. Thus, the PM-state corrected GB energy at 3.666 Å is 1.19 J/m^2 in the PM state (the results are shown in Table II). The calculated GB energy is in reasonable agreement with the existing experimental high-temperature estimate of the GB energy in γ-Fe [44].

D. GB impurity segregation

In this section, we study the GB segregation of B as well as C and N to different interstitial and substitutional sites in the fcc GB, see Fig. 1. In Fig. 5, we show the segregation energies of B, N, and C obtained for the NM GB in fcc Fe at the 0 K equilibrium lattice constant. As one can see, all elements have segregation energy profiles, with a minimum within the GB plane. The strongest segregation tendency is for B, followed by C, and N, although the segregation energy of N is positive, which means that it does not segregate to this particular selected GB. The segregation energy of C is only −0.24 eV, i.e., C weakly segregates to the GB. Both N and C atoms are found to have the interstitial site preference at the GB, whereas B can occupy both interstitial and substitutional GB sites of virtually the same segregation energy of −1.56 eV.

In the previous sections, we have shown that the magnetic contribution related to the high-temperature PM of Fe is relatively small at lattice constants corresponding to the temperature range of the γ phase stability, between 1100 and 1670 K. Since the GB segregation energy of impurity atoms [Eq. (4)] represents the difference between the solution energies of an impurity atom in bulk and at the GB, we can expect that the energy change from NM to PM states obtained in the previous section will mostly cancel out and only local effects of B on the magnetic structure of Fe atoms may be of importance.

To estimate the effect of the PM state on B segregation to the preferred substitutional GB site 0 (see Fig. 1), we have performed an additional set of EMTO calculations using the NM relaxed GB structure from VASP. The obtained magnetic correction is 0.11 eV at the lattice parameter of 3.666 Å. This means that magnetic contribution cannot play a decisive role in the case of B and, besides, the observed differences in the segregation energies between B and the other interstitials in the NM Σ5[100](012) GB can be described fairly well in the NM state. At the same time, C and N segregation energies can be more sensitive to the magnetic effects of the order of 0.11 eV as their segregation energies are relatively small.

If one compares these results to the available experimental data on segregation of B and C in the austenite [11,45–47] (see Fig. 6), one can see that the result for B agrees best with the most recent results from Da Rosa *et al.* [11], who obtained the segregation energy of B in austenite to be −0.39 eV. The results of another experimental investigation by Grabke *et al.* [46] suggest that the segregation energy of B can be as high as −1.04 eV [48]. Given the potential differences in the GB structure (special CSL GB in the calculation and unknown, most likely general GB structure in the experiment) and the fact that only the effective segregation energies are evaluated in the experiment [49], the agreement between theoretical calculations and the experiments looks very reasonable. The PM state correction partly neglects the contribution from the phonons (the lattice expansion effect has been taken into account) and the configuration entropy effects [49] still may change the theoretical value, but we do not expect them to be dominant for the case of B segregation.

The situation is different for C and N segregation. Grabke *et al.* [46] experimentally estimated the segregation energy of C in PM fcc Fe to be −0.31 eV. Our results can confirm the relative difference in the segregation energies between B and C. B has a 30% (0.4 eV) lower segregation energy than C in our calculations vs 40% (0.7 eV) difference in the

measurements, but the calculations predict the antisegregation behavior for C atoms, whereas the experimental study suggests the opposite. Apparently, a substantially lower segregation tendency of C in fcc Fe compared to that of B requires a more detailed and accurate theoretical description. Direct calculations of magnetic and phonon contributions to the segregation energy of the interstitial C can improve the accuracy of the qualitative and quantitative predictions at elevated temperatures. We believe that the same conclusion holds true for N segregation, though we could find no experimental data for comparison to confirm it.

IV. CONCLUSION

Boron solubility and GB segregation in PM fcc Fe has been studied by DFT calculations. The starting point has been the supercell total energy calculations by VASP done in the NM state while the magnetic contribution to the thermodynamics of nonmagnetic fcc Fe has been obtained in the EMTO calculations, which provide quite easy access to the energy of the PM state relative to the that of the NM one.

In order to obtained the solution energies in high temperature γ-Fe, the calculations have been done at the constant theoretical pressure, which corresponds to the high temperature lattice constant. The obtained substitutional and interstitial solution energies of B in the fcc Fe, change very little in the temperature interval between between 0 K and 1183 K where magnetic contribution is quite small in both cases. However, it increases quite dramatically for the substitutional case at the lattice constants corresponding to high temperatures, although it is still below 0.2 eV for the largest lattice constant values within the range of the γ-phase stability.

Calculations of B segregation to the special symmetric CSL $\Sigma5$[100](012) GB revealed that B can segregate to both interstitial and substitutional GB sites with the segregation energy of about -1.5 eV. With lattice expansion corresponding to 1670 K, the segregation energy increases up to -0.3 eV, indicating a weaker segregation tendency, which has been found in line with experimental measurements. The contribution of the PM state to the B segregation energy at this lattice constant has been calculated to be of the order of 0.1 eV.

We have also calculated the segregation energy of C and N to the same GB. We find slightly positive (order of 0.1 eV) segregation energies for both elements. The calculated energy difference between B and C GB segregation energy matched quite well the corresponding energy difference in the experiment, meaning that the applied approach allowed us to capture the qualitative segregation trends between C and B atoms reasonably well.

ACKNOWLEDGMENTS

We acknowledge funding from Christian Doppler Laboratory, No. 1467395. The DFT simulations were performed on resources provided by the Swedish National Infrastructure for Computing (SNIC) at PDC (Stockholm) and NSC (Linköping) and through PRACE resources. We acknowledge PRACE for awarding us access to Piz Daint at CSCS, Switzerland. AVR acknowledges a European Research Council grant, the VINNEX center Hero-m, financed by the Swedish Governmental Agency for Innovation Systems (VINNOVA), Swedish industry, and the Royal Institute of Technology (KTH). A.V.R. also gratefully acknowledges the financial support under the scope of the COMET program within the K2 Center "Integrated Computational Material, Process and Product Engineering (IC-MPPE)" (Project No 859480). This program is supported by the Austrian Federal Ministries for Climate Action, Environment, Energy, Mobility, Innovation and Technology (BMK) and for Digital and Economic Affairs (BMDW), represented by the Austrian research funding association (FFG), and the federal states of Styria, Upper Austria, and Tyrol.

[1] J. Takahashi, K. Ishikawa, K. Kawakami, M. Fujioka, and N. Kubota, Atomic-scale study on segregation behavior at austenite grain boundaries in boron- and molybdenum-added steels, Acta Mater. **133**, 41 (2017).

[2] Y. Li, D. Ponge, P. Choi, and D. Raabe, Atomic scale investigation of non-equilibrium segregation of boron in a quenched mo-free martensitic steel, Ultramicroscopy **159**, 240 (2015), 1st International Conference on Atom Probe Tomography and Microscopy.

[3] L. Karlsson and H. Norden, Grain boundary segregation of boron. an experimental and theoretical study, J. Phys. Colloq. **47**, C7-257 (1986).

[4] S. ichi Komazazki, S. Watanabe, and T. Misawa, Influence of phosphorus and boron on hydrogen embrittlement susceptibility of high strength low alloy steel, ISIJ Int. **43**, 1851 (2003).

[5] A. S. Kholtobina, W. Ecker, R. Pippan, and V. I. Razumovskiy, Effect of alloying elements on hydrogen enhanced decohesion in bcc iron, Comput. Mater. Sci. **188**, 110215 (2021).

[6] M. Kadowaki, A. Saengdeejing, I. Muto, Y. Chen, G. S. Frankel, T. Doi, K. Kawano, Y. Sugawara, and N. Hara, Roles of interstitial nitrogen, carbon, and boron in steel corrosion: Generation of oxyanions and stabilization of electronic structure, J. Electro. Soc. **167**, 081503 (2020).

[7] X. Li, P. Wu, S. Zhao, C. Chen, R. Yin, and N. Chen, First-principle study of the solution type of boron in gamma-iron, Energy Procedia **16**, 661 (2012), 2012 International Conference on Future Energy, Environment, and Materials.

[8] J. Jang, Y. B. Lee, K. T. Kim, Y. K. Kim, and W. S. Ryu, JAERI-Conf 2003-001, in *Proceedings of the 3 International Symposium on Material Chemistry in Nuclear Environment*, Vol. 1 (Japan Atomic Energy Research Institute, Kashiwa, Chiba, Japan, 2003), pp. 77–83.

[9] M. Yamaguchi, First-principles study on the grain boundary embrittlement of metals by solute segregation: Part I. iron (Fe)-solute (B, C, P, and S) systems, Metall. Mater. Trans. A **42**, 319 (2011).

[10] R. Wu, A. J. Freeman, and G. B. Olson, First principles determination of the effects of phosphorus and boron on iron grain boundary cohesion, Science **265**, 376 (1994).

[11] G. Da Rosa, P. Maugis, A. Portavoce, J. Drillet, N. Valle, E. Lentzen, and K. Hoummada, Grain-boundary segregation of boron in high-strength steel studied by nano-SIMS and atom probe tomography, Acta Mater. **182**, 226 (2020).

[12] B. Lüthi, L. Ventelon, D. Rodney, and F. Willaime, Attractive interaction between interstitial solutes and screw dislocations in bcc iron from first principles, Comput. Mater. Sci. **148**, 21 (2018).

[13] L. Q. Chen, Z. C. Qiu, C. Y. Wang, and T. Yu, Electronic effect of boron impurity on the kink in bcc iron, J. Alloys Compd. **428**, 49 (2007).

[14] A. F. Bialon, T. Hammerschmidt, and R. Drautz, *Ab initio* study of boron in α-iron: Migration barriers and interaction with point defects, Phys. Rev. B **87**, 104109 (2013).

[15] S. Ahlawat, K. Srinivasu, A. Biswas, and N. Choudhury, First-principle investigation of electronic structures and interactions of foreign interstitial atoms (C, N, B, O) and intrinsic point defects in body- and face-centered cubic iron lattice: A comparative analysis, Comput. Mater. Sci. **170**, 109167 (2019).

[16] A. V. Ponomareva, Y. N. Gornostyrev, and I. A. Abrikosov, *Ab initio* calculation of the solution enthalpies of substitutional and interstitial impurities in paramagnetic fcc fe, Phys. Rev. B **90**, 014439 (2014).

[17] P. E. Blöchl, Projector augmented-wave method, Phys. Rev. B **50**, 17953 (1994).

[18] G. Kresse and J. Hafner, *Ab initio* molecular dynamics for open-shell transition metals, Phys. Rev. B **48**, 13115 (1993).

[19] G. Kresse and J. Furthmüller, Efficiency of *ab-initio* total energy calculations for metals and semiconductors using a plane-wave basis set, Comput. Mater. Sci. **6**, 15 (1996).

[20] J. P. Perdew, K. Burke, and M. Ernzerhof, Generalized Gradient Approximation Made Simple, Phys. Rev. Lett. **77**, 3865 (1996).

[21] H. J. Monkhorst and J. D. Pack, Special points for brillouin-zone integrations, Phys. Rev. B **13**, 5188 (1976).

[22] A. V. Ruban and V. I. Razumovskiy, Spin-wave method for the total energy of paramagnetic state, Phys. Rev. B **85**, 174407 (2012).

[23] L. Vitos, H. Skriver, B. Johansson, and J. Kollár, Application of the exact muffin-tin orbitals theory: The spherical cell approximation, Comput. Mater. Sci. **18**, 24 (2000).

[24] L. Vitos, Total-energy method based on the exact muffin-tin orbitals theory, Phys. Rev. B **64**, 014107 (2001).

[25] L. Vitos, I. A. Abrikosov, and B. Johansson, Anisotropic Lattice Distortions in Random Alloys from First-Principles Theory, Phys. Rev. Lett. **87**, 156401 (2001).

[26] P. Soven, Coherent-potential model of substitutional disordered alloys, Phys. Rev. **156**, 809 (1967).

[27] B. L. Gyorffy, Coherent-potential approximation for a nonoverlapping-muffin-tin-potential model of random substitutional alloys, Phys. Rev. B **5**, 2382 (1972).

[28] S. He, W. Ecker, O. Peil, R. Pippan, and V. I. Razumovskiy, The effect of solute atoms on the bulk and grain boundary cohesion in ni: Implications for hydrogen embrittlement, Materialia **21**, 101293 (2022).

[29] S. He, M. N. Popov, W. Ecker, R. Pippan, and V. Razumovskiy, A theoretical insight into hydrogen clustering at defects in ni, Philo. Mag. Lett. **101**, 68 (2021).

[30] N. Kulo, S. He, W. Ecker, R. Pippan, T. Antretter, and V. I. Razumovskiy, Thermodynamic and mechanical stability of Ni_3X-type intermetallic compounds, Intermetallics **114**, 106604 (2019).

[31] S. He, W. Ecker, R. Pippan, and V. I. Razumovskiy, Hydrogen-enhanced decohesion mechanism of the special $\Sigma5$ (012)[100] grain boundary in Ni with Mo and C solutes, Comput. Mater. Sci. **167**, 100 (2019).

[32] V. Razumovskiy, A. Lozovoi, and I. Razumovskii, First-principles-aided design of a new Ni-base superalloy: Influence of transition metal alloying elements on grain boundary and bulk cohesion, Acta Mater. **82**, 369 (2015).

[33] D. Scheiber, R. Pippan, P. Puschnig, and L. Romaner, *Ab initio* calculations of grain boundaries in bcc metals, Model. Simul. Mater. Sci. Eng. **24**, 035013 (2016).

[34] D. Scheiber, O. Renk, M. Popov, and L. Romaner, Temperature dependence of surface and grain boundary energies from first principles, Phys. Rev. B **101**, 174103 (2020).

[35] A. S. Ebner, S. Jakob, H. Clemens, R. Pippan, V. Maier-Kiener, S. He, W. Ecker, D. Scheiber, and V. I. Razumovskiy, Grain boundary segregation in ni-base alloys: A combined atom probe tomography and first principles study, Acta Mater. **221**, 117354 (2021).

[36] T. Hajilou, I. Taji, F. Christien, S. He, D. Scheiber, W. Ecker, R. Pippan, V. I. Razumovskiy, and A. Barnoush, Hydrogen-enhanced intergranular failure of sulfur-doped nickel grain boundary: *In situ* electrochemical micro-cantilever bending vs. DFT, Mater. Sci. Eng. A **794**, 139967 (2020).

[37] I. Seki and K. Nagata, Lattice constant of iron and austenite including its supersaturation phase of carbon, ISIJ Int. **45**, 1789 (2005).

[38] I. A. Abrikosov, A. E. Kissavos, F. Liot, B. Alling, S. I. Simak, O. Peil, and A. V. Ruban, Competition between magnetic structures in the fe rich fcc feni alloys, Phys. Rev. B **76**, 014434 (2007).

[39] F. Haglöf, A. Blomqvist, A. Ruban, and M. Selleby, CALPHAD: Method for calculation of finite temperature thermodynamic properties for magnetic allotropes–case study on Fe, Co and Ni, Calphad **74**, 102320 (2021).

[40] I. Bleskov, T. Hickel, J. Neugebauer, and A. Ruban, Impact of local magnetism on stacking fault energies: A first-principles investigation for fcc iron, Phys. Rev. B **93**, 214115 (2016).

[41] X. Zhang, X. Li, P. Wu, S. Chen, S. Zhang, N. Chen, and X. Huai, First principles calculation of boron diffusion in fcc-fe, Curr. Appl. Phys. **18**, 1108 (2018).

[42] T. W. He, Y. H. Jiang, R. Zhoua, and J. Feng, Point defect interactions in iron lattice: A first-principles study, RSC Adv. **6**, 45250 (2016).

[43] Y. Li, C. Han, C. Zhang, K. Jia, P. Han, and X. Wu, Effects of alloying on the behavior of B and S at $\Sigma5(210)$ grain boundary in γ-fe, Comput. Mater. Sci. **115**, 170 (2016).

[44] E. Hondros and N. P. Allen, The influence of phosphorus in dilute solid solution on the absolute surface and grain boundary energies of iron, Proc. R. Soc. Lond. A: Math. Phys. Sci. **286**, 479 (1965).

[45] J. E. Morral and W. F. Jandeska, The binding energy of boron to austenite grain boundaries as calculated from autoradiography, Metal. Trans. A **11**, 1628 (1980).

[46] H. J. Grabke, Surface and grain boundary segregation on and in iron and steels, ISIJ Int. **29**, 529 (1989).

[47] L. Karlsson and H. Nordén, Overview no. 63 non-equilibrium grain boundary segregation of boron in austenitic stainless steel-II. Fine scale segregation behaviour, Acta Metal. **36**, 13 (1988).

[48] M. Paju, H. Viefhaus, and H. J. Grabke, Phosphorus segregation in austenite in Fe-P-C, Fe-P-B and Fe-P-C-B alloys, Steel Res. **59**, 336 (1988).

[49] V. Razumovskiy, S. Divinski, and L. Romaner, Solute segregation in cu: Dft vs. experiment, Acta Mater. **147**, 122 (2018).